REV-scale numerical assessment of metal foam porosity effect on a PCM's melting in a latent heat energy storage unit.

Riheb MABROUK [1*], Hassane NAJI [2], Hacen DHAHRI [1]

[1]Université de Monastir, École Nationale d'Ingénieurs de Monastir, Laboratoire d'Études des Systèmes Thermiques et Énergétiques (LESTE)
Rue Ibn Jazza - 5019 Monastir (Tunisia)
[2]Univ. Artois, IMT Nord Europe, Junia, Univ. Lille, ULR 4515, Laboratoire de Génie Civil et géo-Environnement (LGCgE)
F - 62400 Béthune (France)
[*](Corresponding author: mabroukriheb@gmail.com)

Abstract - This article deals with the numerical investigation of the enhancement of heat transfer under forced convection in an open-ended horizontal channel filled with a porous structure (metal foam) and a phase change material (*PCM: paraffin*). Simulations are done using the thermal Single Relaxation Time (*T-SRT*) lattice Boltzmann Method (*LBM*) at the representative elementary volume (*REV*) scale. Numerical results were performed to present the effects of porosities ($0.5 \le \varepsilon \le 0.9$) on Bejan number and melting front for the sequent *Re* range ($200 \le \mathrm{Re} \le 400$). Based on the results achieved, it can be stated that the melting process under laminar forced convection is speeded up by decreasing the porosity ($\varepsilon = 0.5$).

Nomenclature

Bi	Biot number, $\mathrm{Bi} = h_{sf} a_{sf} H^2 / \lambda_s$
c	lattice speed, $\mathrm{m.s}^{-1}$
C_s	sound speed, $\mathrm{m.s}^{-1}$
Da	Darcy number, $\mathrm{Da} = K.H^{-2}$
Ec	Eckert number, $\mathrm{Ec} = Uo^2 / (C_f . \Delta T_{ref})$
La	latent heat, $\mathrm{J.Kg}^{-1}$
P	dimensionless pressure
Pr	Prandtl number, $\mathrm{Pr} = \nu_f / \alpha_f$
Rc	heat capacity ratio, $\mathrm{Rc} = (\rho C_p)_s / (\rho C_p)_f$
Re	Reynolds number
Ste	Stefan number, $\mathrm{Ste} = C_p (T_h - T_m) / L_a$
T	temperature, K
$\vec{U}$	dimensionless velocity along the X-direction
w_i	equilibrium weighting coefficients
X, Y	dimensionless coordinates

Greek symbols

λ	thermal conductivity, $\mathrm{W.m}^{-1}.\mathrm{K}^{-1}$
ν	kinematic viscosity, $\mathrm{m}^2.\mathrm{s}^{-1}$
ρ	density, $\mathrm{kg.m}^{-3}$
ε	porosity
$\tilde{t}$	dimensionless time
τ	dimensionless relaxation time
Θ	dimensionless temperature

Superscripts/subscripts

c	cold
eff	effective
f	fluid
o	inlet
h	hot
ref	reference
s	solid

1. Introduction

Latent Heat Thermal Energy Storage (*LHTES*) tools present the safest and largest mode in storing thermal energy due to its huge energy stored quantity in a small volume for a long time. It is a technique based on the phase transition process of a phase change material (*PCM*) at a nearly constant temperature. Nevertheless, most pure PCMs have a low thermal

https://doi.org/10.25855/SFT2022-089

conductivity which limits their use [1]. Thereby, one of the solutions proposed to enhance their thermal conductivities is the technique of incorporating PCMs into porous structures [2]. Indeed, it is now accepted that the high thermal conductivity of the porous structure and large interfacial surface areas inside porous materials are responsible for improving the heat transfer rate inside the system. A part from that, thermal performance improvement depends on the morphology and characteristics of the porous material such as porosity and pore density [3]. To this end, Sardari *et al.* [4] reported a numerical study dealing with porosity and pore size effects of porous metal foams on a PCM's phase change. They found that small porosities speed up the melting phenomenon by 85% compared to pure PCM while improving system performance. Yang *et al.* [5] investigated a novel latent heat storage (LHS) unit including porous metal foams with positive and negative gradients in pore parameters to improve thermal performance. They stated that the positive porosity gradient design reduces melting time by about 18%, while a 36% increase is achieved with a negative design. Additionally, porosities of 0.89, 0.95 and 0.98 reduce melting time by approximately 21%. Li *et al.* [6] examined the effect of metal foam porosity and nanoparticle concentration on an LHS system via a physical and numerical model. Authors found that the addition of 95% porous metal foam accelerates the melting/solidification time by 84-88%. Mabrouk *et al.* [7] have numerically investigated the porosity and pore density influence on the PCM melting/solidifying processes. They pointed out that small pore density (= 10) mitigates the system irreversibility during melting process, while a large value (=60) is recommended during solidifying period. In addition, high porosity (= 0.9) reduces the system instability.

The main aim here is to numerically study the effect of porosity of a porous matrix and of the Re number on the PCM phase change in the cases of charging and discharging using the single relaxation time (SRT)-LBM supplemented with the enthalpy method at the REV scale. In addition, the effects of viscous forces on energy storage unit and its performance in the both processes are deemed. Then, the system's irreversibility is investigated via emerging parameters.

The remainder of this paper is as follows: After Section 1 (introduction), the physical and mathematical models are described in section 2. Then, in Section 3, the numerical method (LBM) and validation are exposed. In Section 4, the results are discussed. Finally, Section 5 (conclusion) sums the main outcomes.

2. Physical and mathematical system

2.1. Problem setup

The physical system investigated is the one depicted in Figure 1. It is a planar channel with height H and length L (with L=7H) where forced convection fluid flow takes place while being filled with a porous metallic foam and a phase change material (paraffin). Its upper and lower walls are adiabatic and non-slip. During the melting process (charging), the air enters the channel through its pores at a high temperature T_h and a uniform velocity U_0. After heat exchange, the paraffin starts to melt which reduces its volume, then the fluid leaves the channel through the east wall with lower constant temperature T_c. Inversely, during the solidifying process (discharging), the cold air evolves (from right to left) with T_c and the velocity $-U_0$. So, the melted PCM starts to solidify by releasing its energy and thereby, the air heats up to leave the channel at hot temperature T_h.

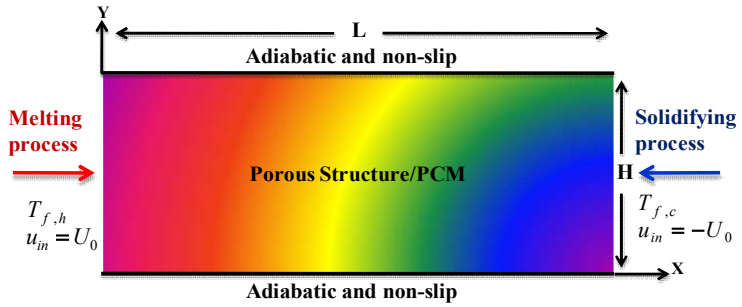

Figure 1: *Schematic display of the physical system*

2.2. Key assumptions

The following conjectures used to simplify the mathematical system resolution are: Fluid flow is laminar, steady, Newtonian and incompressible. The thermo-physical characteristics of the fluid and solid phases are assumed to be constant. The porous medium is saturated, homogeneous and isotropic. The fluid and solid phases are in local thermal non equilibrium (LTNE) condition showing that the viscous dissipation is involved.

2.3. Mathematical system

Under the up-specified assumptions, the governing equations for mass, momentum and energy can be written in dimensionless form at the REV scale as follows [8-10]:

$$\nabla \cdot \vec{U} = 0 \tag{1}$$

$$\frac{\partial \vec{U}}{\partial \tilde{t}} + \left(\vec{U}.\nabla\right)\left(\varepsilon^{-1}\vec{U}\right) = -\nabla\left(\varepsilon P\right) + Re^{-1}\nabla^2\vec{U} - \varepsilon.\underbrace{\left(\frac{1}{Re\,Da} + \frac{F_\varepsilon}{\sqrt{Da}}\left\|\vec{U}\right\|\right)\vec{U}}_{\vec{F}} \tag{2}$$

$$\frac{\partial \Theta_f}{\partial \tilde{t}} + \vec{U}.\nabla\Theta_f = \frac{1}{Re.Pr}\nabla.\left(\frac{\lambda_{eff,f}}{\lambda_f}\nabla\left(\frac{\Theta_f}{\varepsilon}\right)\right) + Kr.\frac{Bi}{Re.Pr}\left(\frac{\Theta_s - \Theta_f}{\varepsilon}\right) - \frac{1}{Ste}\frac{\partial \tilde{\Gamma}}{\partial \tilde{t}} + \tilde{\Phi} \tag{3}$$

$$\frac{\partial \Theta_s}{\partial \tilde{t}} = \frac{Kr}{Rc}\frac{1}{Re.Pr}\nabla.\left(\frac{\lambda_{eff,s}}{\lambda_s}\nabla\left(\frac{\Theta_s}{1-\varepsilon}\right)\right) - \frac{Kr}{Rc}.\frac{Bi}{Re.Pr}\left(\frac{\Theta_s - \Theta_f}{1-\varepsilon}\right) \tag{4}$$

with

$$\tilde{\Phi} = \varepsilon.Ec\left\{\frac{1}{Da.Re} + \frac{F_\varepsilon}{\sqrt{Da}}\left\|\vec{U}\right\|\right\}\left\|\vec{U}\right\|^2 + \frac{Ec}{Re}\left\{2\left[\left(\frac{\partial \vec{U}}{\partial X}\right)^2 + \left(\frac{\partial \vec{V}}{\partial Y}\right)^2\right] + \left(\frac{\partial \vec{U}}{\partial Y} + \frac{\partial \vec{V}}{\partial X}\right)^2\right\} \tag{5}$$

and

$$\tilde{\Gamma} = \begin{cases} 0 & \\ \dfrac{\Theta - \Theta_s}{\Theta_l - \Theta_s} & if \\ 1 & \end{cases} \quad \begin{array}{l} \Theta < \Theta_s \\ \Theta_s \le \Theta \le \Theta_f \\ \Theta > \Theta_f \end{array} \tag{6}$$

The main dimensionless variables deemed here are expressed as follows:

$$(X,Y)=(x,y)/H, U=u/U_0, P=p/\rho U_0^2, \tilde{t}=tU_0/H, \Theta=(T-T_c)/(T_h-T_c), \Delta T_{ref}=T_h-T_c,$$
$$Da=K/H^2, Pr=\nu_f/\alpha_f, Re=U_{in}H/\nu_f, Rc=(\rho C_p)_s/(\rho C_p)_f, Kr=\lambda_s/\lambda_f, \quad (7)$$
$$Bi=h_{sf}a_{sf}H^2/\lambda_s, Ste=C_{pf}(T_h-T_m)/La, Ec=U_0^2/\left(C_f\Delta T_{ref}\right)$$

where $\vec{U}$, P, $\Theta_{f/s}$, ε, $\vec{F}$, $\tilde{\Gamma}$, λ, $\tilde{\Phi}$ and λ_e denote the velocity vector filed, the pressure, the fluid/solid temperatures, metal foam porosity, the total force due to porous media and other external forces, the PCM's liquid fraction, the thermal conductivity, the viscous dissipation and equivalent thermal conductivity, respectively. Subscripts f and s represent the fluid and solid phases, respectively.

2.4. LTNE intensity

The LTNE criterion is calculated via the following parameter [8], to name a few:

$$LTNE=\sum_N\left|\Theta_s-\Theta_f\right|/N \quad (8)$$

where N represents the total number of nodes (= 480x120 in this study).

Note that, if $\mathrm{LTNE}>5\%$, the LTNE condition should be applied and if $\mathrm{LTNE}<5\%$, the local thermal equilibrium (LTE) condition prevails between phases.

2.5. Bejan number

To deal with the system's instability, Bejan number (Be) assessed the origin of the irreversibility which is due either by heat transfer irreversibility (HTI) or by fluid friction irreversibility (FFI). Note that Be ranges from 0 to 1 and whose expression is [8]:

$$Be=HTI/\left(HTI+FFI\right) \quad (9)$$

where

$$HTI=\frac{\varepsilon}{(\Theta_f+\Pi)^2}\left[\left(\frac{\partial\Theta_f}{\partial X}\right)^2+\left(\frac{\partial\Theta_f}{\partial Y}\right)^2\right]+\frac{(1-\varepsilon)Kr}{\left(\Theta_s+\Pi\right)^2}\left[\left(\frac{\partial\Theta_s}{\partial X}\right)^2+\left(\frac{\partial\Theta_s}{\partial Y}\right)^2\right]+\frac{Bi.Kr(\Theta_s-\Theta_f)^2}{(\Theta_f+\Pi)(\Theta_s+\Pi)}, \quad (10)$$

$$FFI=\frac{Ec.Pr}{\left(\Theta_f+\Pi\right)}\left[2\left(\left(\frac{\partial\vec{U}}{\partial X}\right)^2+\left(\frac{\partial\vec{V}}{\partial Y}\right)^2\right)+\left(\frac{\partial\vec{U}}{\partial Y}+\frac{\partial\vec{V}}{\partial X}\right)^2\right]+\frac{\varepsilon.Ec.Pr}{\left(\Theta_f+\Pi\right)}\left(\frac{1}{Da}+\frac{Re.F_\varepsilon}{\sqrt{Da}}\left\|\vec{U}\right\|\right)\left\|\vec{U}\right\|^2$$

3. Lattice Boltzmann method (LBM)

In this work, the mathematical system (Eqs. (1)-(4)) is shaped through the single relaxation time (SRT) scheme (also called Bhatnagar-Gross-Krook (BGK)). Under the LTNE condition, the SRT-lattice Boltzmann equation (SRT-LBE) has been applied with three distribution functions for dynamic ($f_i(x,t)$) and thermal ($g_{i,f,s}(x,t)$) fields to handle the particles evolution at time t positioned at x. Thereby, the SRT-LBEs at the REV scale can be given as [9, 11]:

$$\underbrace{f_i\left(\vec{x}+\vec{e}_i\delta t,t+\vec{e}_i\delta t\right)-f_i\left(\vec{x},t\right)}_{stream}=-\delta t\underbrace{\left(f_i\left(\vec{x},t\right)-f_i^{eq}\left(\vec{x},t\right)\right)}_{collision\ term}/\tau_v+\delta t.\ \underbrace{\vec{F}_{e_i}}_{force\ term} \quad (11)$$

$$\underbrace{g_{f,i}\left(\vec{x}+\vec{e}_i\delta t,t+\delta t\right)-g_{f,i}\left(\vec{x},t\right)}_{streaming}=\underbrace{-\left(g_{f,i}\left(\vec{x},t\right)-g_{f,i}^{eq}\left(\vec{x},t\right)\right)/\tau_{T,f}}_{collision\ term}+\underbrace{\left(1+\delta t\partial_t/2\right)\delta tSr_{i,f}+\delta tf_i\left(\vec{x},t\right)q_i}_{source\ terms} \tag{12}$$

$$\underbrace{g_{s,i}\left(\vec{x}+\vec{e}_i\delta t,t+\delta t\right)-g_{s,i}\left(\vec{x},t\right)}_{streaming}=\underbrace{-\left(g_{s,i}\left(\vec{x},t\right)-g_{s,i}^{eq}\left(\vec{x},t\right)\right)/\tau_{T,s}}_{collision\ term}+\underbrace{\left(1+\delta t\partial_t/2\right)\delta tSr_{i,s}}_{source\ term} \tag{13}$$

Under the D2Q9 model, the local equilibrium distribution functions $f_i^{eq}\left(\vec{x},t\right)$ and $g_{i,f;s}^{eq}$ can be expressed as follows [9, 11]:

$$f_i^{eq}=\rho w_i\left(1+\frac{\vec{e}_i.\vec{u}}{c_s^2}+\frac{\vec{u}\otimes\vec{u}:\left(\vec{e}_i\otimes\vec{e}_i-c_s^2I\right)}{2c_s^4\varepsilon}\right) \tag{14}$$

$$g_{f,i}^{eq}=w_iT_f\left(1+e_iu/(\varepsilon c_s^2)\right)\ and\ \ g_{s,i}^{eq}=w_iT_s \tag{15}$$

where the particle streaming velocity ($\vec{e}_i$) and the equilibrium weighting coefficients (w_i) are expressed as follows:

$$\vec{e}_i=\begin{cases}0\vec{i}+0\vec{j}, & i=0\\ c\left(\cos\theta_i\vec{i}+\sin\theta_i\vec{j}\right),\ \theta_i=(i-1)\pi/2 & i=1,2,3,4\\ \sqrt{2}c\left[\cos\theta_i\vec{i}+\sin\theta_i\vec{j}\right],\ \theta_i=(2i-9)\pi/4 & i=5,6,7,8\end{cases} \tag{16}$$

$$w_i=\begin{cases}4/9 & i=0\\ 1/9 & i=1,2,3,4\\ 1/36 & i=5,6,7,8\end{cases} \tag{17}$$

The source terms in Eq. (11) - (13) are calculated as [9, 11]:

$$\overrightarrow{F_{e_i}}=w_i\rho(1-\frac{1}{2\tau_v})\left[\frac{\vec{e}_i.\vec{F}}{c_s^2}+\frac{\vec{u}.\vec{F}:\left(\vec{e}_i\vec{e}_i-c_s^2I\right)}{\varepsilon c_s^4}\right] \tag{18}$$

$$Sr_{i,f}=w_i\left(\frac{La}{C_{p,f}}\left[\frac{\gamma(t+\delta t)-\gamma(t)}{\delta t}\right]+\frac{h(T_s-T_f)}{\varepsilon(\rho C_p)_f}\right) \tag{19}$$

$$Sr_{i,s}=w_i\left(\frac{h(T_s-T_f)}{(1-\varepsilon)(\rho C_p)_s}\right) \tag{20}$$

$$q_i=-(f_i-f_i^{eq})(\vec{e}_i-\vec{u})(\vec{e}_i-\vec{u}):\Delta\vec{u} \tag{21}$$

Finally, the macroscopic quantities $\rho,\vec{u},T_f,T_s$ are computed as follows:

$$\rho=\sum_i f_i,\quad \rho\vec{u}=\sum_i f_i\vec{e}_i+\delta t\vec{F}/2,\ T_f=\sum g_{fi}\ and\ \ T_s=\sum g_{si} \tag{22}$$

3.1. Validation step

Figure 2 portrays a comparison of the LTNE intensity at two axial positions X=0.14 and X=0.5 obtained by our in-house code with results of Abdedou *et al.* [12].

Through this figure, it can be observed a good agreement between results thereby, indicating the reliability of our in-house code based on the LB approach.

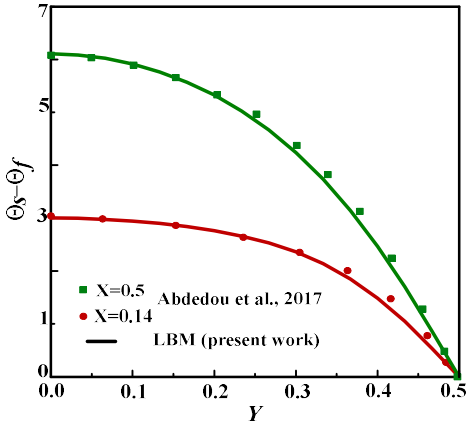

Figure 2: *LTNE intensity* ($\Theta_s - \Theta_f$) *vs. dimensionless transverse distance Y for* $Da = 10^{-4}, Bi = 0.01, Re = 100 = Rq$ *and* $Kr = 1$

4. Results

4.1. Porosity effect on LTNE condition

Figure 3 demonstrates the effects of the porosity on the LTNE intensity for Re =200 and 400 during the melting and solidifying periods. As seen, it turned out that the LTNE condition is valid ($\mathrm{LTNE} > 5\%$). It is observable that the LTNE criterion decreases with the porosity increase. Herein, findings are exhibited for $Pr = 50, Bi = 0.1, Ste = 1, Ec = 5, Kr = 10^{+3}$ and $Rc = 1$.

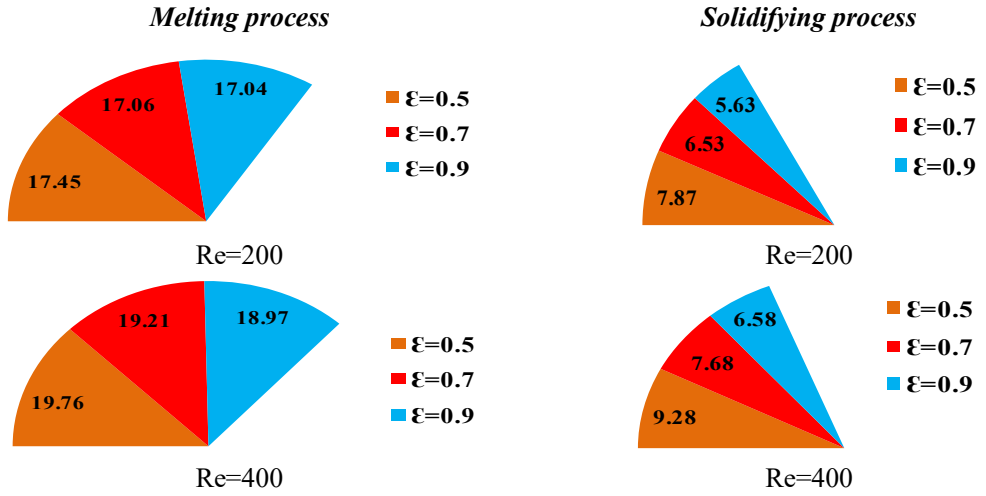

Figure 3: *LTNE criterion during melting and solidifying vs.* ε *set by Re*

4.2. Porosity effect on Bejan number

Effects of Re and porosity on the number of Be vs. Y during the during melting (charging) and solidifying (discharging) processes are shown in Figure 4 at X=0.5 (channel middle). As seen, during both periods, Be exhibits an almost "plateau" profile along the channel (except at the entrance and exit) while being below 0.5 indicating that the FFI dominates the overall system irreversibility due to the high viscous forces and the low system's permeability. As for the inlet and outlet of the channel, the HTI and FFI together affect the system instability due to the temperature gradient change in these areas. On the other hand, porosity has little influence on Be during both processes, while increasing Re reduces the FFI effect. This explains the main role of interfacial heat transfer to ensure the stability of the system.

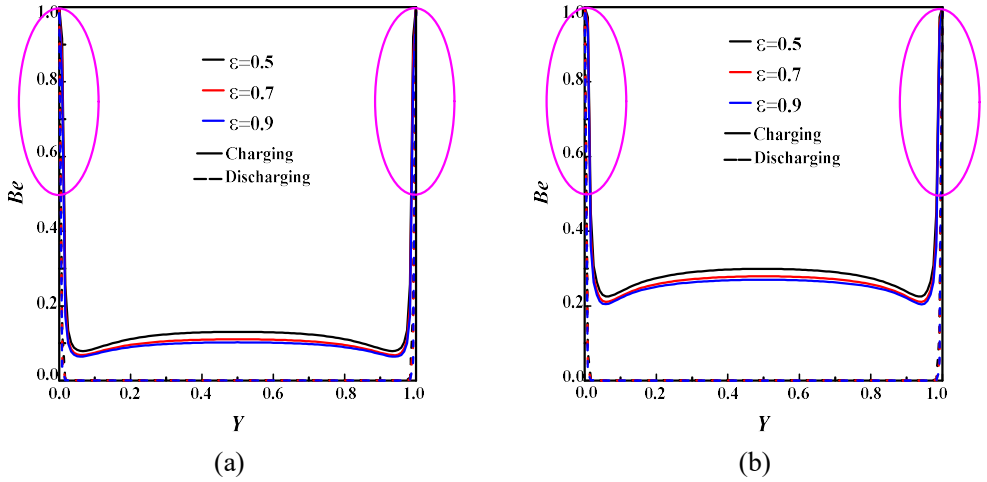

Figure 4: *Porosity and two Re numbers effects on the Bejan number (Be) during melting and solidifying processes; a) Re=200, b) Re=400.*

4.3. Porosity effect on melt front

The panels in Figure 5 depict the porosity effect on the time melt front progression for Re = 400. The red and blue areas indicate the melted and solidified paraffin, while the other colors represent the mushy zone. It is found that the decrease in the porosity accelerates the melting speed owing to the permeability effect of the porous metal foam. Moreover, for a large Re (=400), the interfacial heat transfer between phases intensifies due to the heat transfer dominance that reduces the viscous effects in the pores. In addition, it turned out that a large Re value and a low porosity enhance the system's thermal performances while allowing to store the maximum of energy in a short time.

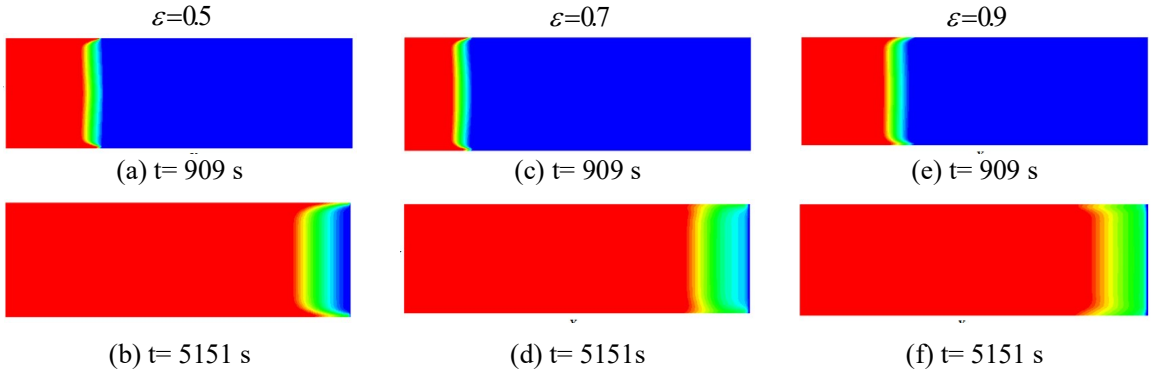

Figure 5: *Porosity effect on melt front (Γ) evolvement at various times during melting period Re=400*

5. Conclusion

The present work reported on the porosity and Re number effects on forced convective heat transfer in a filled porous metal foam/paraffin rectangular channel. The simulations have been performed using the SRT-TLBM approach at the REV scale. The main findings of this study can be summed up as follows:

The LTNE condition is valid during the melting and solidifying periods regardless the parameters deemed.

- Low porosity value accelerates the paraffin melting rate.
- The viscous forces dominate the system's irreversibility.
- Large Re number mitigates the fluid friction irreversibility.

References

[1] X. Huang, X. Chen, A. Li, D. Atinafu, H. Gao, W. Dong, G. Wang, Shape-stabilized phase change materials based on porous supports for thermal energy storage applications, *Chem. Eng. Sci.*, 356 (2019), 641-661.

[2] P. K. S. Rathore, S. K. Shukla, Potential of macro encapsulated PCM for thermal energy storage in buildings: A comprehensive review. *Constr. Build. Mater.*, 225 (2019), 723-744.

[3] G. Alva, L. Liu, X. Huang, G. Fang, Thermal energy storage materials and systems for solar energy applications. *Renew. Sust. Energ. Rev.*, 68 (2017), 693-706.

[4] P.T. Sardari, H.I. Mohammed, D. Giddings, M. Gillott, D. Grant, Numerical study of a multiple-segment metal foam-PCM latent heat storage unit: Effect of porosity, pore density and location of heat source, *Energy*, 189 (2019), 116108.

[5] X. Yang, P. Wei, X. Wang, Y. L. He, Gradient design of pore parameters on the melting process in a thermal energy storage unit filled with open-cell metal foam. *Appl. Energy*, 268 (2020), 115019.

[6] Z. Li, A. Shahsavar, A. A. Al-Rashed, P. Talebizadehsardari, Effect of porous medium and nanoparticles presences in a counter-current triple-tube composite porous/nano-PCM system. *Appl. Therm. Eng.*, 167 (2020), 114777.

[7] R. Mabrouk, H. Naji, H. Dhahri, Z. Younsi, On Numerical Modeling of Thermal Performance Enhancementof a Heat Thermal Energy Storage System Using a Phase Change Material and a Porous Foam. *Computation*, 10(1) (2022), 3.

[8] R. Mabrouk, H. Naji, H. Dhahri, S. Hammouda, Z. Younsi, Numerical investigation of porosity effect on a PCM's thermal performance in a porous rectangular channel via thermal lattice Boltzmann method. *Int. Commun. Heat Mass Transf.*, 153 (2020), 119606.

[9] R. Mabrouk, H. Dhahri, H. Naji, S. Hammouda, Z. Younsi, Lattice Boltzmann simulation of forced convection melting of a composite phase change material with heat dissipation through an open-ended channel, *Int. J. Heat Mass Transf.*, 153 (2020), 119606.

[10] G.F. Al-Sumaily, M.C. Thompson, Forced convection from a circular cylinder in pulsating flow with and without the presence of porous media, *Int. J. Heat Mass Transf.*, 61 (2013), 226-244.

[11] Y. B. Tao, Y. You, Y. L. He, Lattice Boltzmann simulation on phase change heat transfer in metal foams/paraffin composite phase change material, *Appl. Therm. Eng.*, 93 (2016), 476-485.

[12] A. Abdedou, K. Bouhadef, R. Bennacer, Forced convection in a self-heating porous channel: local thermal non-equilibrium model, *Therm. Sci.*, 21 (6A) (2017), 2413-2423.

Acknowledgements

The authors are grateful to the Artois University for its support of this work through the study internships achieved at the Civil Engineering & Geo-Environment Laboratory.